

Article

# A Corrected Adaptive Balancing Approach of Motorized Spindle Considering Air Gap Unbalance

Hongwei Fan <sup>1,2,3,\*</sup>, Jin Wang <sup>3,\*</sup>, Sijie Shao <sup>1</sup>, Minqing Jing <sup>3</sup>, Heng Liu <sup>3</sup> and Xuhui Zhang <sup>1,2</sup>

<sup>1</sup> School of Mechanical Engineering, Xi'an University of Science and Technology, Xi'an 710054, China; 15686427553@163.com (S.S.); zhangxh@xust.edu.cn (X.Z.)

<sup>2</sup> Shaanxi Key Laboratory of Mine Electromechanical Equipment Intelligent Monitoring, Xi'an 710054, China

<sup>3</sup> School of Mechanical Engineering, Xi'an Jiaotong University, Xi'an 710049, China; mjing@mail.xjtu.edu.cn (M.J.); hengliu@mail.xjtu.edu.cn (H.L.)

\* Correspondence: hw\_fan@xust.edu.cn (H.F.); wangjin@cs48.com (J.W.); Tel.: +86-1999-125-6906 (H.F.); +86-1378-731-1152 (J.W.)

Received: 5 February 2020; Accepted: 16 March 2020; Published: 24 March 2020

**Featured Application:** The corrected adaptive balancing approach considering air gap unbalance can mainly be used for the precision motorized spindle of high-end machine tools.

**Abstract:** Motorized spindles widely used for high-speed precision machine tools are very sensitive to the mass unbalance of rotors; thus, their balancing problem is always a research hotspot. Although many significant studies were done regarding the theory and application of various rotor balancing technologies for motorized spindles, the particularity of motorized spindles is not carefully considered in the existing balancing approaches. When the rotor unbalance of a motorized spindle occurs in operation, it is subject to both the mass unbalance-induced inertia force and air gap unbalance-induced electromagnetic force, which is an important feature that distinguishes the motorized spindle from a mechanical spindle. This paper describes an investigation into the corrected adaptive balancing approach of a motorized spindle by newly introducing a coefficient representing the removing effect of the air gap unbalance of the motor on the balancing capacity into the balancing formula. The determination of the newly defined coefficient refers to the calculation of electromagnetic force caused by the dynamic air gap eccentricity of motor; thus, much attention is paid to the analytical derivation of the unbalanced magnetic pull (UMP). Finally, a motorized spindle with an electromagnetic ring balancer was developed; then, the balancing tests and vibration signal analysis were done to validate the effectiveness of the newly proposed balancing approach in residual vibration reduction. It can be seen from the test results under different cases that the proposed balancing approach is effective.

**Keywords:** motorized spindle; air gap unbalance; unbalanced magnetic pull (UMP); adaptive balancing; balancing test

---

## 1. Introduction

High-speed precision machining [1] is an important direction of modern cutting technology. Spindle [2] is the key functional part of a cutting machine, and the rotating unit which is made up of tool, holder, and shaft has a direct effect on the workpiece quality. For the spindle of a machine tool, vibration is an important factor that affects its rotary accuracy. Vibration of a machine tool spindle in machining generally presents as self-excited vibration and forced vibration. Chatter [3–6] is a typical form of self-excited vibration, and its modeling, prediction, and control were widely studied. Rotor unbalance-induced vibration is a typical form of forced vibration, and much attention was also paid to unbalance correction [7]. Moreover, uneven thermal drift can also cause vibration of machine tool

spindles; thus, the thermal analysis and error compensation of spindles are also important topics [8,9]. In this paper, the control problem of rotor unbalance for a machine tool motorized spindle is discussed.

Motorized spindle [10] is a direct drive spindle, which integrates spindle and motor into one element, eliminating the intermediate transmission link; thus, motorized spindles are widely used for high-speed precision cutting machines. However, the high-speed feature also renders motorized spindle more sensitive to rotor unbalance caused by design, machining, assembly, and cutting. Due to tool wear [11], breakage, change, and so on, mass distribution unbalance of a shaft–holder–tool combined rotor often happens in engineering practice, which firstly causes the spindle to vibrate violently [12] and then has a severe impact on the workpiece surface quality and spindle service life. It can be seen that there were two main research aspects regarding spindle balancing technology; one involved the balancing method and the other involved a balancing device. The balancing methods mainly include the modal balancing method [13], the influence coefficient method (ICM) [14], and magnetic levitation method [15]. The modal balancing method relies on the accurate dynamics calculation of a rotor, while ICM can avoid complicated calculations and it is easy to carry out on a computer; finally, magnetic bearing cannot directly compensate for the unbalanced mass. The balancing devices mainly include the balancing machine, field balancing instrument, and online balancing system. The on-balancing machine balance [16] and on-site balance by a portable instrument [17] are both off-line balancing modes, which need to interrupt the machining process. On-line balancing does not require stopping or human intervention, which allows automatically achieving the precision balancing of spindles. Online balancing systems can be divided into passive [18] and active balancing systems. Passive balancing is realized by automatic matching of dynamics characteristics of balancer and spindle, which has no controller but requires dynamics design. Active balancing is based on the on-line signal analysis and a balancing algorithm, and the balancer is driven by a controller. The active balancing technology has wider applicability for various rotors compared to passive balancing. Therefore, research on the combined use of ICM and active balancer is currently a hot topic for the on-line balancing of machine tool spindles.

As early as 1964, Vegte [19] proposed a mechanical automatic balancer that moved within a Cartesian coordinate system. Since then, a variety of polar-coordinate solid counterweight balancers were studied, including the radial steel ball movement-type structure [20] and electromagnetic ring-type structure [21]. In addition, some scholars also studied active balancing technology using a liquid counterweight [22]. For the active balancing method, Gosiewski [23,24] initially described the theory and implementation, thereby influencing many subsequent balancing methods. Moon [25] developed an ICM-based on-line active electromagnetic ring balancing system for high-speed spindles. Dyer [26] studied an ICM-based single-plane adaptive electromagnetic ring balancing system. Kim [27] investigated the stability of an ICM-based active electromagnetic ring balancing system. Dyer [28] implemented an ICM-based robust multiple-plane active electromagnetic ring balancing. Fan [21,29–32] revealed the design principle of an electromagnetic ring balancer and the influence of control parameters on the adaptive balancing method, developed an adaptive balancing controller, and experimentally studied the dynamics and thermal performance of a motorized spindle with a single electromagnetic ring balancer. These above researches are the representative achievements of on-line active balancing technology of machine tool spindles. However, they did not consider the unique characteristic of rotor unbalance for a motorized spindle. When a motorized spindle is subject to rotor unbalance, the motor of spindle causes uneven air gap distribution between the stator and rotor, thereby producing an extra undesired magnetic pull. The magnetic pull and magnetic vibration for three-phase asynchronous motors were widely studied [33,34], but the air gap eccentricity was never been considered in the active balancing scheme of motorized spindles using a three-phase asynchronous motor, which leads to an inescapable balancing capacity reduction for an online active balancing system.

This paper focuses on a corrected adaptive balancing approach for motorized spindles by eliminating the effect of air gap eccentricity. Firstly, the rotor unbalance of motorized spindle is introduced, and then the air gap unbalance is proposed and the electromagnetic force caused by air

gap unbalance is derived. Then, an ICM-based adaptive balancing method for motorized spindles is defined, where the effect of air gap unbalance-induced electromagnetic force on the active balancing is considered. Finally, the balancing tests and vibration analysis of a specific motorized spindle are carried out to prove the effectiveness of the proposed approach.

## 2. Unbalance and Force of Motorized Spindle

### 2.1. Mechanical Unbalance and Force

When mechanical unbalance is discussed, the stator of motor for a motorized spindle is not considered, and the combined rotor composed of a shaft, holder, and tool is the main research object. As shown in Figure 1, for the combined rotor of a shaft, holder, and tool, the mass unbalance in cutting process mainly appears in this tool due to the inevitable tool wear, breakage, and change, and the cutting tool can be reduced to a circular plane because of its small axial size.

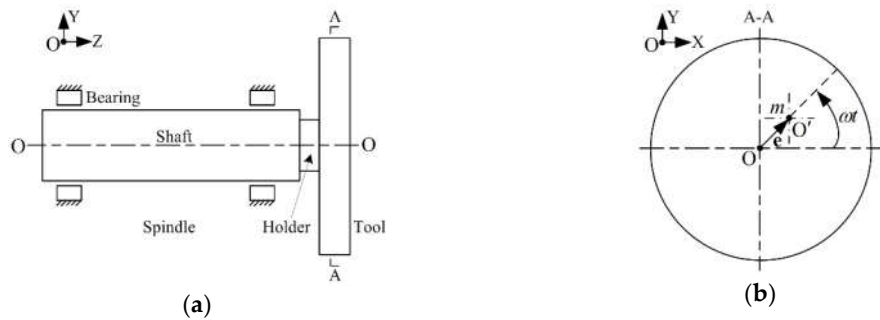


**Figure 1.** Schematic diagram of a combined rotor and its mass unbalance for a motorized spindle: (a) combined rotor of shaft, holder, and tool; (b) mass unbalance of tool.

In Figure 1, assuming that the tool in the A–A plane generates a mass eccentric vector  $m\mathbf{e}$ , the mechanical unbalance vector  $\mathbf{U}$  can be shown as

$$\mathbf{U} = m\mathbf{e} = M\mathbf{e}' \tag{1}$$

where  $m$  is the eccentric mass, and  $\mathbf{e}$  is the position vector of  $m$  in polar coordinates,  $M$  is the total mass of a combined rotor,  $\mathbf{e}'$  is the equivalent eccentricity vector of the combined rotor.

When the motorized spindle rotor is operating at the angular speed of  $\omega$ ,  $\mathbf{U}$  causes an undesired inertia force  $\mathbf{F}$ , which can be expressed as

$$\mathbf{F} = \omega^2\mathbf{U} \tag{2}$$

The force vector  $\mathbf{F}$  can be decomposed and converted into two components of  $F_x$  and  $F_y$  along the horizontal and vertical directions in the Cartesian coordinate system.

$$\begin{cases} F_x = m\omega^2 \cos \omega t \\ F_y = m\omega^2 \sin \omega t \end{cases} \tag{3}$$

According to Equation (3), the unbalance-induced force components are characterized by a frequency equal to the rotating angular frequency  $\omega$ , which causes the mechanical vibration of the spindle system.

### 2.2. Electromagnetic Unbalance and Force

#### 2.2.1. Characteristic of Spindle Motor with Dynamic Air Gap Eccentricity

As a kind of motor, the air gap eccentricity of motorized spindle is inevitable. When the dynamic air gap eccentricity of a spindle motor occurs, the rotor of motor orbits around the geometric axis of the stator.

As shown in Figure 2, it is known that the rotor orbits around the geometric center “O” of stator under the dynamic air gap eccentricity;  $\delta(\theta, t)$  is the air gap length between the motor rotor and stator in a polar coordinate system, which can be represented as follows according to the geometric relationship:

$$\delta(\theta, t) = \delta_0 - \delta_d \cdot \cos(\theta - \omega_r t) , \tag{4}$$

where  $\delta_0$  is the nominal air gap length,  $\delta_d$  is the dynamic air gap eccentricity length,  $\theta$  is the mechanical angle, and  $\omega_r$  is the angular speed at minimum air gap position, expressed as

$$\omega_r = \omega_1(1 - s) / p , \tag{5}$$

where  $p$  is the magnetic pole pair number of motor,  $s$  is the motor slip rate, and  $\omega_1$  is the angular frequency of motor power supply.

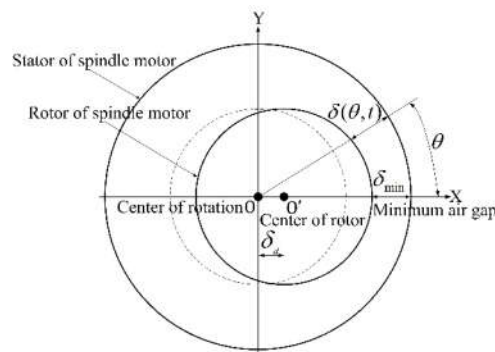


Figure 2. Schematic diagram of dynamic air gap unbalance for the motor of a motorized spindle.

When a motorized spindle is subject to the dynamic air gap eccentricity, the unbalanced magnetic pull (UMP) of the motor is generated, causing an undesired electromagnetic vibration of the spindle rotor. If the UMP contains  $1 \times$  rotating frequency component, then  $1 \times$  rotating frequency component of the UMP should be removed from the balancing reference of the online active balancing scheme in frequency domain to improve the balancing effect. Therefore, the key problem is the calculation of the UMP. For different types of motors, the UMP calculations are different. This paper mainly applies a three-phase asynchronous spindle motor driven by a frequency converter to calculate the UMP.

### 2.2.2. Calculation Scheme of Electromagnetic Force of Spindle Motor

According to the literature [34,35], the electromagnetic force of a three-phase asynchronous spindle motor can be calculated using the Maxwell stress tensor (MST) method; the flow chart of the calculation process of MST is shown in Figure 3.

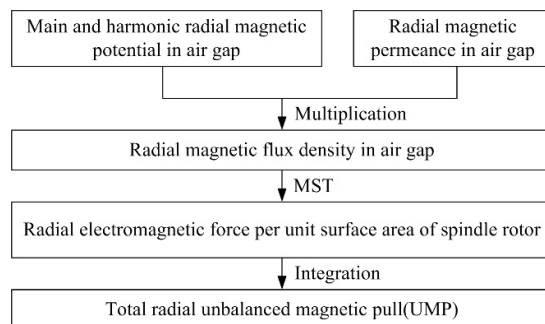


Figure 3. Electromagnetic force solving process of spindle motor.

Firstly, the radial magnetic flux density in the air gap is obtained by multiplying the main magnetic potential and high-order harmonic magnetic potential in the air gap between the stator and rotor along the radial direction with the air gap permeability. Then, the radial electromagnetic force per unit surface area of the spindle rotor is calculated using the MST method. Finally, the analytical expression of the total radial electromagnetic force is obtained by integrating the radial electromagnetic force on the unit surface area of rotor.

### 2.2.3. Electromagnetic Force of Spindle Motor without Eccentricity

Firstly, for an asynchronous motorized spindle with three-phase symmetrical windings, the resultant radial magnetic potential can be expressed as

$$f(\theta, t) = f_p(\theta, t) + \sum_v f_v(\theta, t) + \sum_\mu f_\mu(\theta, t), \quad (6)$$

where

$$f_p(\theta, t) = F_p \cos(p\theta - \omega_1 t - \varphi_0), \quad (7)$$

$$f_v(\theta, t) = F_v \cos(v\theta - \omega_1 t - \varphi_v), \quad (8)$$

$$f_\mu(\theta, t) = F_\mu \cos(\mu\theta - \omega_\mu t - \varphi_\mu), \quad (9)$$

where  $f_p(\theta, t)$ ,  $f_v(\theta, t)$ , and  $f_\mu(\theta, t)$  are the main magnetic potential, the harmonic magnetic potential of the stator, and the harmonic magnetic potential of the rotor, respectively, while  $v$  and  $\mu$  are the harmonic orders of the stator and rotor, respectively.

Secondly, the radial magnetic permeance can be approximated as

$$\lambda(\theta, t) = \Lambda_0 + \sum_{k_1} \lambda_{k_1} + \sum_{k_2} \lambda_{k_2}, \quad (10)$$

where  $\Lambda_0$  is the invariant part of permeance,  $\lambda_{k_1}$  is the harmonic permeance caused by the stator slots,  $\lambda_{k_2}$  is the harmonic permeance caused by the rotor slots, and both  $\lambda_{k_1}$  and  $\lambda_{k_2}$  are numerically very small and can be ignored.

Thirdly, according to Equations (6) and (10), the instantaneous radial magnetic density can be derived as

$$b(\theta, t) = f(\theta, t)\lambda(\theta, t) = B_1 \cos(p\theta - \omega_1 t - \varphi_0) + \sum_v B_v \cos(v\theta - \omega_1 t - \varphi_v) + \sum_\mu B_\mu \cos(\mu\theta - \omega_\mu t - \varphi_\mu), \quad (11)$$

where  $B_1$  is the main magnetic density amplitude, while  $B_v$  and  $B_\mu$  are the harmonic magnetic density amplitudes of stator and rotor, respectively.

Finally, the radial electromagnetic force generated by the air gap magnetic field and acting on the unit surface area of rotor is proportional to the square of the radial magnetic flux density in the air gap; the radial electromagnetic force on the unit surface area of spindle rotor can be approximated as

$$P_r(\theta, t) = \frac{b^2(\theta, t)}{2\mu_0}, \quad (12)$$

where  $\mu_0$  is the vacuum permeability, and  $\mu_0 = 4\pi \times 10^{-7}$  H/m.

As the electromagnetic force with lower order and larger amplitude plays a major role in the vibration level of the spindle rotor, the higher-order and smaller-amplitude components of the radial electromagnetic force are omitted, and the constant components are omitted; thus, it can be obtained that the radial electromagnetic force per unit surface area of spindle rotor is

$$p_r(\theta, t) = \frac{1}{2\mu_0} \left\{ \frac{B_1^2}{2} \cos(2p\theta - 2\omega_1 t - 2\varphi_{0r}) + \sum_{\nu_2} \sum_{\mu_2} B_{\nu_2} B_{\mu_2} \cos[(\mu \pm \nu)\theta - (\omega_\mu \pm \omega_\nu)t - (\varphi_\mu \pm \varphi_\nu)] \right\} \tag{13}$$

The integral operation of Equation (13) is obtained as

$$\begin{cases} F_{\text{cmx}} = LR \int_0^{2\pi} p_r(\theta, t) \cos\theta d\theta \\ F_{\text{cm y}} = LR \int_0^{2\pi} p_r(\theta, t) \sin\theta d\theta \\ F_{\text{cm}} = \sqrt{F_x^2 + F_y^2} \end{cases}, \tag{14}$$

where  $F_{\text{cmx}}$  and  $F_{\text{cm y}}$  are two components of the electromagnetic force along the horizontal and vertical directions in the Cartesian coordinate system, respectively,  $F_{\text{cm}}$  is their resultant force, and  $L$  and  $R$  are the length and radius of the spindle rotor, respectively. For the case with no eccentricity, according to Equations (13) and (14), the spindle is not subject to UMP, i.e.,  $F_{\text{cm}} = 0$ .

#### 2.2.4. UMP of Spindle Motor with Dynamic Air Gap Eccentricity

In the case of dynamic air gap eccentricity, the air gap permeability can be expressed as

$$\Lambda_s(\theta) = \Lambda_0(1 + \varepsilon' \cos(\theta - \omega_r t)), \tag{15}$$

where  $\varepsilon'$  is the relative air gap eccentricity ratio, defined as  $\varepsilon' = \delta_d / \delta_0$ .

By substituting Equation (15) into Equation (11), it is obtained that

$$\begin{aligned} b(\theta, t) = f(\theta, t)\lambda(\theta, t) = & B_1 \cos(p\theta - \omega_1 t - \varphi_0) + \sum_{\nu} B_{\nu} \cos(\nu\theta - \omega_{\nu} t - \varphi_{\nu}) + \sum_{\mu} B_{\mu} \cos(\mu\theta - \omega_{\mu} t - \varphi_{\mu}) + \\ & \frac{\varepsilon'}{2} B_1 \cos[(p \pm 1)\theta - (\omega_1 \pm \omega_r)t - \varphi_0] + \frac{\varepsilon'}{2} \sum_{\nu} B_{\nu} \cos[(\nu \pm 1)\theta - (\omega_{\nu} \pm \omega_r)t - \varphi_{\nu}] + \frac{\varepsilon'}{2} \sum_{\mu} B_{\mu} \cos[(\mu \pm 1)\theta - (\omega_{\mu} \pm \omega_r)t - \varphi_{\mu}] \end{aligned} \tag{16}$$

where the first three terms are the air gap magnetic fields without eccentricity, and the last three terms are the additional magnetic fields produced by dynamic air gap eccentricity.

By substituting Equation (16) into Equation (12), we get

$$\begin{aligned} p_r(\theta, t) = & \frac{1}{2\mu_0} \left\{ \frac{B_1^2}{2} \cos(2p\theta - 2\omega_1 t - 2\varphi_0) + \frac{B_1^2 \varepsilon'}{2} \cos[(p \pm (p \pm 1))\theta - (\omega_1 \pm (\omega_1 \pm \omega_r))t - (\varphi_0 \pm \varphi_0)] + \right. \\ & \sum_{\nu} \sum_{\mu} B_{\nu} B_{\mu} \cos[(\mu \pm \nu)\theta - (\omega_{\mu} \pm \omega_{\nu})t - (\varphi_{\mu} \pm \varphi_{\nu})] + \sum_{\nu} B_{\nu}^2 \frac{\varepsilon'}{2} \cos[(\nu \pm (\nu \pm 1))\theta - (\omega_{\nu} \pm (\omega_{\nu} \pm \omega_r))t - (\varphi_{\nu} \pm \varphi_{\nu})] + \\ & \sum_{\nu} \sum_{\mu} B_{\nu} B_{\mu} \varepsilon' \cos[(\mu \pm 1) \pm \nu)\theta - ((\omega_{\mu} \pm \omega_r) \pm \omega_{\nu})t - (\varphi_{\mu} \pm \varphi_{\nu})] + \\ & \left. \sum_{\mu} B_{\mu}^2 \frac{\varepsilon'}{2} \cos[(\mu \pm (\mu \pm 1))\theta - (\omega_{\mu} \pm (\omega_{\mu} \pm \omega_r))t - (\varphi_{\mu} \pm \varphi_{\mu})] \right\} \end{aligned} \tag{17}$$

According to Equation (17), under dynamic air gap eccentricity, the rotor is subjected to the following low-order electromagnetic forces:

i) First-order and  $2p \pm 1$ -order low-frequency radial electromagnetic force produced by the interaction of the  $p \pm 1$ -order harmonic with the main magnetic field, the frequencies of which are  $\omega_r$  and  $2\omega_1 \pm \omega_r$ , respectively.

ii)  $\mu \pm \nu \pm 1$ -order high-frequency radial electromagnetic force produced by the interaction of the  $\mu \pm 1$ -order harmonic with the tooth harmonic magnetic field of the stator and the interaction of the  $\nu \pm 1$ -order harmonic with the tooth harmonic magnetic field of the rotor, the frequencies of which are  $\omega_{\mu} \pm \omega_r \pm \omega_{\nu}$ .

iii) First-order low-frequency radial electromagnetic force produced by the interaction of the  $\nu \pm 1$ -order harmonic and the tooth harmonic magnetic field of the stator, the frequency of which is  $\omega_r$ .

iv) First-order low-frequency radial electromagnetic force produced by the interaction of the  $\mu \pm 1$ -order harmonic and the tooth harmonic magnetic field of the rotor, the frequency of which is  $\omega_r$ .

### 2.2.5. Main Component of UMP Affecting the Balancing Capacity

The ZYS-170MD12Y16 motorized spindle used in this paper is a four-pole three-phase asynchronous frequency conversion motor; thus, its rotation speed is calculated by

$$n = \frac{60f_1}{p} = 30f_1, \tag{18}$$

where  $f_1$  is the frequency of the motor power supply.

Then, the rotating frequency of spindle is obtained by

$$f_r = \frac{n}{60} = 0.5f_1. \tag{19}$$

According to Equations (13) and (17), the order and frequency of the electromagnetic forces were calculated, as listed in Table 1; since the high-order forces cause a low-level vibration, the electromagnetic forces over the fourth order were ignored.

**Table 1.** Electromagnetic forces of ZYS-170MD12Y16 motorized spindle under no eccentricity and dynamic air gap eccentricity.

Electromagnetic Force (EF)	No Eccentricity		Dynamic Eccentricity	
	Order	Frequency	Order	Frequency
EF caused by main magnetic field	4	$2f_1$	4	$2f_1$
EF caused by interaction of the tooth harmonic magnetic fields of the stator and rotor	0	$12f_1$	0	$12f_1$
	4	$14f_1$ $26f_1$	4	$14f_1$ $26f_1$
EF caused by interaction of the main and $p \pm 1$ -order harmonic magnetic field	None		1	$0.5f_1$
			3	$1.5f_1$
EF caused by interaction of the stator tooth harmonic and $\mu \pm 1$ -order harmonic magnetic field	None		1	$11.5f_1$
				$12.5f_1$
			3	$13.5f_1$ $25.5f_1$
EF caused by interaction of the rotor tooth harmonic and $\mu \pm 1$ -order harmonic magnetic field	None		1	$0.5f_1$
EF caused by interaction of the rotor tooth harmonic and $\nu \pm 1$ -order harmonic magnetic field	None		1	$11.5f_1$
				$12.5f_1$
			3	$13.5f_1$ $25.5f_1$
EF caused by interaction of the stator tooth harmonic and $\nu \pm 1$ -order harmonic magnetic	None		1	$0.5f_1$

field

It can be seen from Table 1 that the first-order 1× rotation frequency electromagnetic forces (EFs) were caused by dynamic air gap eccentricity, which consists of three parts including the EF caused by interaction of the main and  $p \pm 1$ -order harmonic field, the EF caused by interaction of the rotor tooth harmonic and  $\mu \pm 1$ -order harmonic field, and the EF caused by interaction of the stator tooth harmonic and  $\nu \pm 1$ -order harmonic field. Furthermore, the components of the first-order 1× rotation frequency electromagnetic forces are listed in Table 2, which represent the main components of the UMP affecting the frequency-domain balancing capacity; MFD is shorthand for magnetic flux density.

**Table 2.** The 1× rotation frequency components of electromagnetic forces under dynamic air gap eccentricity. MFD—magnetic flux density.

Order of EF	First Order of MFD	Second Order of MFD	Order Number of EF	Frequency
$p \pm (p \pm 1)$	2	1	1	$0.5f_1$
		3	1	$0.5f_1$
$\nu \pm (\nu \pm 1)$	$\nu$	$\nu - 1$	1	$0.5f_1$
		$\nu + 1$	1	$0.5f_1$
$\mu \pm (\mu \pm 1)$	$\mu$	$\mu - 1$	1	$0.5f_1$
		$\mu + 1$	1	$0.5f_1$

### 2.2.6. Quantitative Relationship between Unbalanced Mechanical and Electromagnetic Forces

According to Table 2, for the same order formula of electromagnetic forces, two first-order 1× rotation frequency components are obtained; thus, Equation (17) can be simplified as Equation (20).

$$p_n(\theta, t) = \frac{\varepsilon'(B_1^2 + \sum_{\nu} B_{\nu}^2 + \sum_{\mu} B_{\mu}^2)}{2\mu_0} \cos(\theta - \omega, t) . \tag{20}$$

Substituting Equation (20) into Equation (14), we get

$$\begin{cases} F_{\text{emx}} = \frac{LR(B_1^2 + \sum_{\mu} B_{\mu}^2 + \sum_{\nu} B_{\nu}^2)\pi\varepsilon'}{2\mu_0} \cos \omega, t \\ F_{\text{emy}} = \frac{LR(B_1^2 + \sum_{\mu} B_{\mu}^2 + \sum_{\nu} B_{\nu}^2)\pi\varepsilon'}{2\mu_0} \sin \omega, t \\ F_{\text{em}} = \sqrt{F_x^2 + F_y^2} = \frac{LR(B_1^2 + \sum_{\mu} B_{\mu}^2 + \sum_{\nu} B_{\nu}^2)\pi\varepsilon'}{2\mu_0} \end{cases} . \tag{21}$$

For the squirrel-cage motor, its rotor has a compensation effect for the uneven magnetic field; thus, the UMP shown in Equation (21) is corrected by adding an empirical coefficient  $\chi$  [35,36] as follows:

$$F_{\text{em}} = \frac{\chi LR(B_1^2 + \sum_{\mu} B_{\mu}^2 + \sum_{\nu} B_{\nu}^2)\pi\varepsilon'}{2\mu_0} . \tag{22}$$

Therefore, in the case of dynamic air gap eccentricity, the rotor is pulled by an unbalanced electromagnetic force with the frequency of 1× rotating frequency, the direction of UMP from the rotation center of the rotor to the minimum air gap position is changing, and the amplitude of force is proportional to the dynamic air gap eccentricity.

According to Equations (2) and (22), we can define a coefficient  $k$ .

$$k = \frac{F_{em}}{F + F_{em}}, \tag{23}$$

where  $k$  represents the quantitative relationship between the unbalanced mechanical and electromagnetic forces, which is used for the correction of the adaptive balancing method.

### 3. Adaptive Balancing Approach of Motorized Spindle

#### 3.1. Conventional Adaptive Balancing Method

According to the literature [26,30], a single-plane adaptive balancing algorithm of a motorized spindle rotor based on the online influence coefficient estimation was built, with the iterative equation shown in Equation (24).

$$\varsigma_{k+1} = \varsigma_k - \alpha \frac{U_k}{\hat{c}_k}, \tag{24}$$

where  $\varsigma_i$  is the product of balancing mass and its radius generated by the active balancer at the  $i$ -th trial,  $U_i$  is the  $1 \times$  rotation frequency vibration component of the rotor system at the  $i$ -th trial,  $\alpha$  is the gain factor of rotor system, usually  $0 < \alpha < 1$  (a small gain factor can improve the balancing stability, but reduce the convergence rate, and vice versa), and  $\hat{c}_i$  is the online estimated influence coefficient of rotor system at the  $i$ -th trial.

$$\hat{c}_k = (1 - \lambda)c_{k-1} + \lambda c_k, \tag{25}$$

where  $\lambda$  is the forgetting factor, usually  $0 \leq \lambda \leq 1$  (a small forgetting factor can improve the anti-interference ability of balancing process, and a large forgetting factor can make the balancing process converge quickly), and  $c_i$  is the actual influence coefficient.

$$c_i = \frac{U_i - U_{i-1}}{\varsigma_i - \varsigma_{i-1}}. \tag{26}$$

#### 3.2. Corrected Adaptive Balancing Method

When the electromagnetic unbalance effect of a spindle motor is considered, the balancing iterative formula is corrected as

$$\varsigma_{k+1} = \varsigma_k - \alpha \frac{U_k}{\hat{c}'_k}, \tag{27}$$

where  $\hat{c}'_k$  is defined as

$$\hat{c}'_k = \tau \hat{c}_k = (1 - k)\hat{c}_k, \tag{28}$$

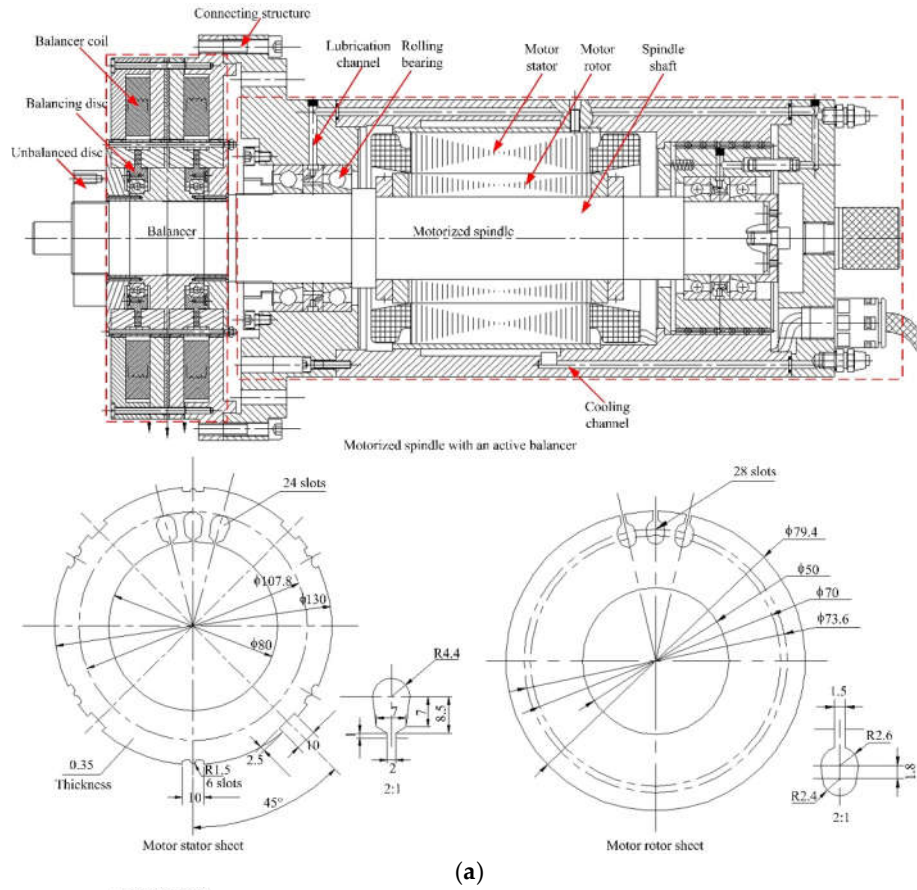
where  $\tau$  is defined as the ratio of the rotor mass unbalance-induced inertia force  $F$  to the total  $1 \times$  rotation frequency force  $F + F_{em}$ ,  $\tau = 1 - k$ , and  $0 < \tau < 1, 0 < k < 1$ .

It can be seen that in essence the introduction of  $\tau$  or  $k$  makes the estimated value of influence coefficient more approximate to the real situation. For the above adaptive balancing equation, when the amplitude of vibration is greater than the preset threshold value, the balancing program is automatically started, otherwise the balancing process stops immediately.

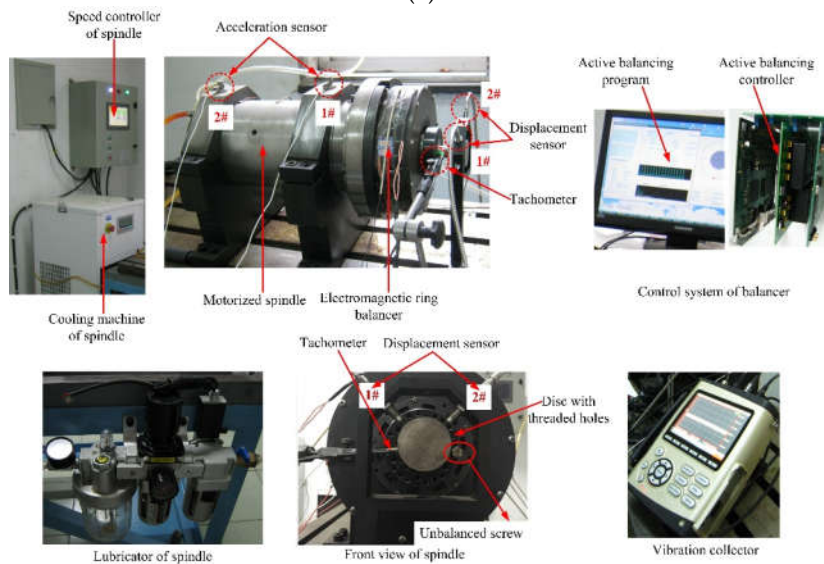
## 4. Experiments

4.1. Motorized Spindle and Its Test Bed

The ZYS-170MD12Y16 motorized spindle with a single electromagnetic ring balancer was designed and developed, as shown in Figure 4. Figure 4a shows the design results of the motorized spindle with a balancer, rotor, and stator sheet of the spindle motor, while Figure 4b shows the developed prototype of the motorized spindle and adaptive electromagnetic ring balancing system. The main parameters of the balancer–spindle system are listed in Table 3.



(a)



(b)

**Figure 4.** ZYS-170MD12Y16 motorized spindle and its active balancing test system: (a) design of a motorized spindle with a balancer and its stator and rotor; (b) prototype of motorized spindle with a balancer and its monitoring and control system.

**Table 3.** Main design parameters of ZYS-170MD12Y16 motorized spindle.

Parameter	Value	Parameter	Value
Outer diameter of stator (mm)	130	Outer diameter of rotor (mm)	79.4
Inner diameter of stator (mm)	80	Inner diameter of rotor (mm)	50
Length of stator core (mm)	110	Length of rotor core (mm)	112
Number of stator slots	24	Number of rotor slots	28
Pair number of magnetic poles	2	Length of air gap (mm)	0.3
Phase number of motor	3	Natural frequency of spindle rotor (Hz)	586.7 [37]
Total mass of balancer–spindle rotor (kg)	12.649	Maximum balancing capacity of balancer (g·cm)	38.55

As shown in Figure 4, the motorized spindle system was composed of a motorized spindle, speed controller, cooling machine, and lubricator, while a metal disc with threaded holes was mounted onto the front end of the spindle rotor to generate unbalance. The active balancing system was composed of a balancer, controller and control program, tachometer, and acceleration and displacement sensors, whereby the balancer offsets the unbalance vector of the spindle rotor via the vector synthesis of two polar coordinate-type counterweights driven by the electromagnetic force of ring coils [21,29]. Moreover, a portable vibration collector was used for the real-time collection of signals from those sensors, i.e., the vibration signals were divided into the balancing controller and the external vibration acquisition instrument.

Two piezoelectric sensors mounted on the front and rear bearing housings were used to collect the vertical acceleration-type vibration signals, two orthogonal eddy current sensors radially mounted on a support located around the perimeter of the unbalanced disc were used to collect the radial displacement-type vibration signals, and an optical fiber tachometer was used to collect the real-time rotation speed of motorized spindle and detect the unbalance phase. The digital signal processor (DSP) TMS320C6713PYP-based active balancing controller and the Microsoft visual studio (MVS)-based balancing control program were developed by the authors [31]. The active balancing control system mainly realizes the functions of vibration signal analysis, adaptive balancing control algorithm execution, and balancer drive. The main parameters of both kinds of vibration sensors used are shown in Table 4.

**Table 4.** Main parameters of two kinds of vibration sensors.

Kind	Type	Linear Range	Sensitivity
Acceleration sensor	Dytran3255A6	± 25 g	200 mV/g
Displacement sensor	JX20	0.5–1.5 mm	4 V/mm

#### 4.2. Calculation of Balancing Correction Coefficient

Using the above design parameters, Equation (22), and the electromagnetics calculation [35], the 1× rotation frequency component of the UMP for the ZYS-170MD12Y16 motorized spindle was obtained to be

$$F_{em} = 5.6709 \times 10^4 \chi \delta_d . \quad (29)$$

According to Equation (2), the 1× rotation frequency inertia force is

$$F = me\omega^2 = 12.649e'\omega^2 . \tag{30}$$

Therefore, according to Equation (23), the ratio of the 1× rotation frequency UMP and the total 1× rotation frequency force is expressed as

$$k = \frac{5.6709 \times 10^4 \chi \delta_d}{12.649e'\omega^2 + 5.6709 \times 10^4 \chi \delta_d} . \tag{31}$$

where  $\chi=0.63$  [35], because of the uncertainty of the axial distribution of dynamic air gap eccentricity, the Equation (31) was simplified according to the pretest. In this paper, the equivalent value  $\delta_d^{eq}$  of dynamic air gap eccentricity  $\delta_d$  is approximated as  $\delta_d^{eq}=e'$ , this moment, it can be seen that the correction coefficient  $k$  is related to the square of angular velocity [35].

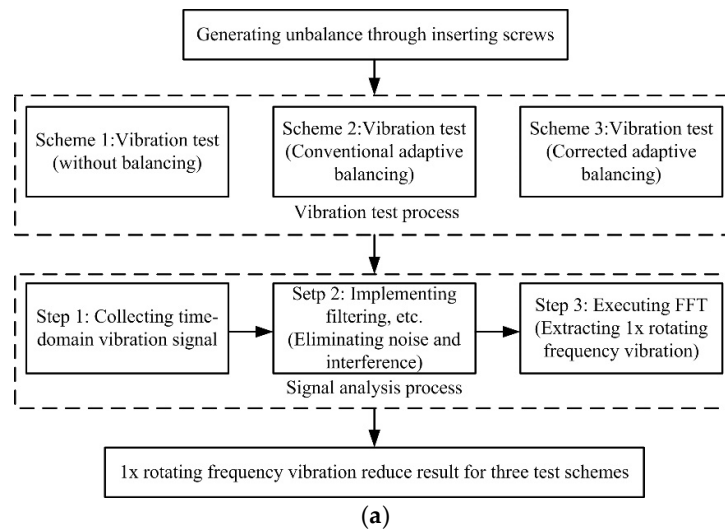
#### 4.3. Experiment Design and Signal Analysis Scheme

In order to validate the newly corrected adaptive balancing approach for motorized spindles, the balancing tests were done for two typical unbalance cases. The unbalanced mass and its vector position are listed in Table 5. Two kinds of unbalance vectors were realized by inserting counterweight screws into the threaded holes of the metal disc, as shown in Figure 4. In addition, the tested rotation speeds were set by the frequency converter below 3000 rpm, including four speeds of 1500 rpm, 1800 rpm, 2100 rpm, and 2400 rpm.

**Table 5.** Unbalanced mass and its position used for the balancing test.

Case	Unbalanced mass $m(g)$	Phase( $^\circ$ )	Vector radius $e(mm)$
Case 1	4.5	0	36
Case 2	9.0	180	

The whole vibration test and the signal analysis scheme used in this paper are shown in Figure 5.



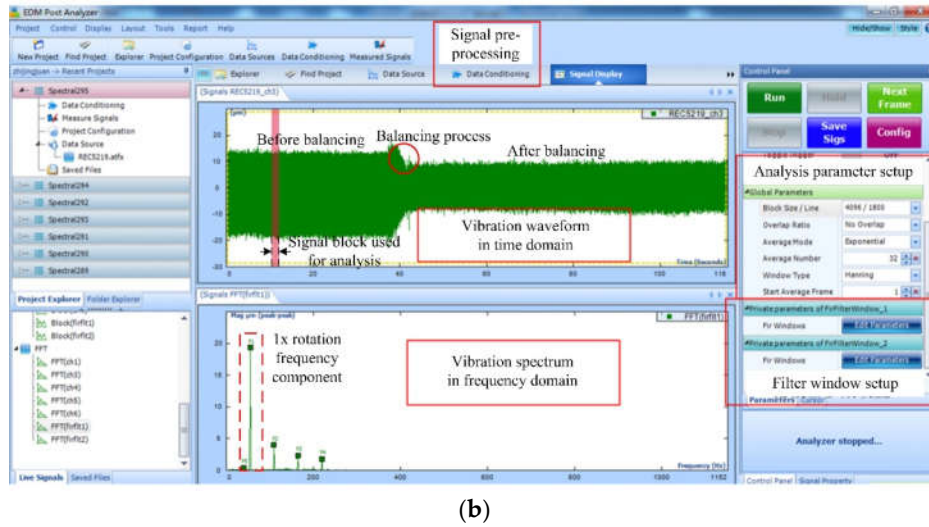


**Figure 5.** Vibration test and analysis flow chart for balancing purpose: (a) the whole test scheme; (b) vibration signal analysis scheme.

As shown in Figure 5a, by inserting the counterweight screws into the threaded holes of the metal disc, the rotor unbalance of the motorized spindle was generated. For four different rotation speeds, three kinds of vibration tests were successively carried out, including a vibration test before balancing, a vibration test with conventional adaptive balancing [26,30], and a vibration test with the newly corrected adaptive balancing considering the effect of UMP in this paper. For each kind of test, the collected original vibration signals firstly underwent pre-processing as filtering, and then the 1× rotating frequency vibration component was extracted using the fast Fourier transform (FFT) algorithm [38], where FFT can transform the vibration signals at the constant speeds from time domain to frequency domain. It can be seen from Figure 5b that FFT surely obtains all frequency components of the tested vibration signals, and the 1× rotation frequency vibration component is found to be a maximum peak compared to the other frequency components.

4.4. Results and Discussion

For the above experiment designs, tests and analyses were performed. The results are shown in Figure 6 and Figure 7, where the horizontal coordinate is the rotation speed and the vertical coordinate is the 1× rotation frequency vibration amplitude. We give the 1× rotation frequency vibrations from the #2 displacement sensor (a more sensitive channel to rotor unbalance-induced vibration than the #1 displacement sensor) and the #2 acceleration sensor (less disturbed than the #1 acceleration sensor), where the unit of the (acceleration signal is the gravitational acceleration ( $g = 9.8 \text{ m/s}^2$ )).

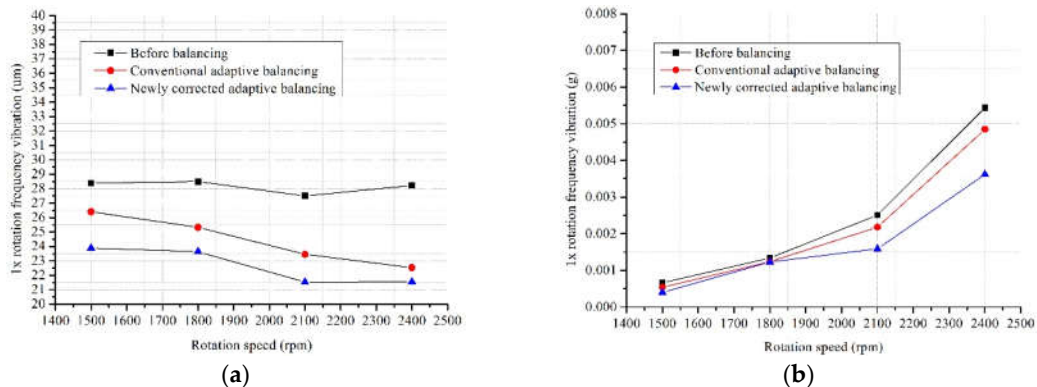


**Figure 6.** Balancing results for Case 1: (a) #2 displacement sensor; (b) #2 acceleration sensor.

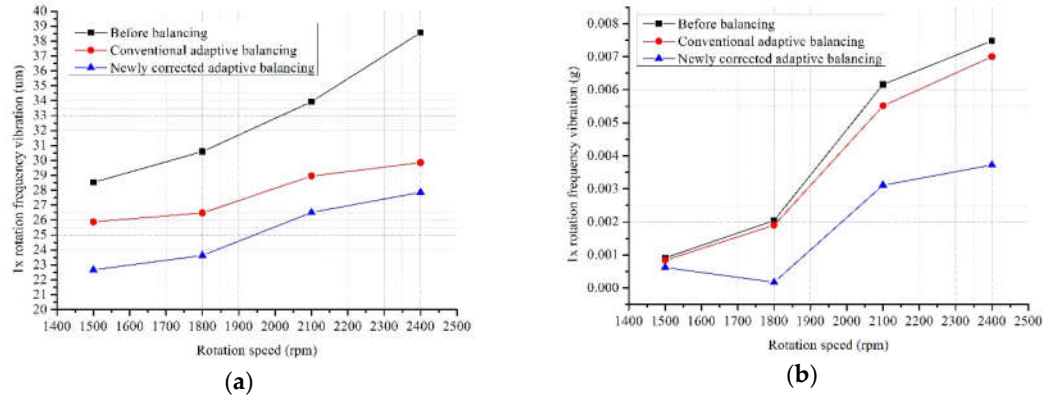


Figure 7. Balancing results for Case 2: (a) #2 displacement sensor; (b) #2 acceleration sensor.

According to Figure 6 and Figure 7, by comparing the three dotted lines in each figure, it can be known that the conventional (marked by “•”) and newly corrected (marked by “▲”) adaptive balancing approaches using a single electromagnetic ring balancer surely reduce the 1× rotation frequency vibration level caused by the rotor unbalance of the motorized spindle, regardless of the displacement or acceleration signal. When the newly corrected balancing approach proposed in this paper was applied, the residual 1× rotation frequency vibration level after balancing was further reduced compared to the conventional method without considering the effect of UMP. The reduction rates of the 1× rotation frequency vibration at different speeds using the conventional and corrected methods are summarized in Table 6.

Table 6. Vibration reduction rate using the proposed method compared to conventional method.

Case 1								
	Displacement (um)				Acceleration (g)			
Speed (rpm)	1500	1800	2100	2400	1500	1800	2100	2400
Before balancing	28.39	28.50	27.50	28.23	0.00066	0.00134	0.00251	0.00544
Conventional method	26.40	25.32	23.46	22.53	0.00054	0.00124	0.00218	0.00485
Reduction rate I (%)	7.00	11.16	14.69	20.19	18.18	7.46	13.15	10.85
Proposed method	23.89	23.64	21.53	21.54	0.00040	0.00123	0.00159	0.00362
Reduction rate II (%)	15.85	17.05	21.71	23.70	39.39	8.21	36.65	33.46
Rate difference (%)	8.85	5.89	7.02	3.51	21.21	0.75	23.50	22.61
Average (%)	6.32				17.02			
Case 2								
	Displacement (um)				Acceleration (g)			
Speed (rpm)	1500	1800	2100	2400	1500	1800	2100	2400
Before balancing	28.53	30.59	33.93	38.56	0.00091	0.00204	0.00616	0.00748
Conventional method	25.88	26.48	28.95	29.85	0.00084	0.00190	0.00551	0.00700
Reduction rate I (%)	9.29	13.44	14.68	22.59	7.69	6.86	10.55	6.42
Proposed method	22.66	23.63	26.51	27.86	0.00062	0.00017	0.00311	0.00372
Reduction rate II (%)	20.57	22.75	21.87	27.75	31.87	91.67	49.51	50.27
Rate difference (%)	11.28	9.31	7.19	5.16	24.18	84.81	38.96	43.85
Average (%)	8.24				47.95			

In Table 6, the vibration reduction rates I and II, as well as the difference of the two reduction rates and the average of rate difference values at four speeds, are defined by Equations (32), (33), and (34).

$$\xi_I = \frac{v_I - v_0}{v_0}, \quad \xi_{II} = \frac{v_{II} - v_0}{v_0}, \tag{32}$$

$$\Delta\xi = \xi_{II} - \xi_I, \tag{33}$$

$$\overline{\Delta\xi} = \frac{\sum_{i=1}^n (\Delta\xi)_i}{n}, n = 4, \tag{34}$$

where  $v_i$  is the  $1\times$  rotation frequency vibration before balancing ( $i = 0$ ), using the conventional method ( $i = I$ ), and using the proposed method in this paper ( $i = II$ ),  $\xi_i$  is the relative vibration reduction rate to vibration before balancing using the conventional method ( $i = I$ ) and proposed method in this paper ( $i = II$ ),  $\Delta\xi$  is the difference between  $\xi_I$  and  $\xi_{II}$ , and  $\overline{\Delta\xi}$  is average of  $\Delta\xi$  for the same sensor and unbalance vector.

As seen in Table 6, the corrected method proposed in this paper improved the vibration reduction rate by a maximum value  $(\Delta\xi)_{\max}$  of 84.81% and a maximum average value  $(\overline{\Delta\xi})_{\max}$  of 47.95%, and the variation law of vibration reduction rates is not linear. The data in Table 6 show that the newly proposed adaptive balancing approach considering the air gap unbalance is effective for the improvement of the active balancing capacity of a motorized spindle, which positively contributes to high-speed precision machine tools.

### 5. Conclusions

The original intention of this work was to improve the existing rotor adaptive balancing method by considering the effect of air gap unbalance on the balancing scheme, which is an interesting topic for motorized spindles. In order to achieve this goal, we made the following assumptions and simplifications: (i) a single-plane balancing strategy was adopted to mainly reduce the tool unbalance in the machining process, which is an approximation to the tool-holder-shaft combined rotor; (ii) the influence coefficient method (ICM) and the frequency-domain analysis of vibration signals were adopted, which are based on the assumption that the spindle system runs smoothly; however, in practice, the non-stationary factors affect the balancing effect; (iii) in the calculation of unbalanced magnetic pull (UMP), the  $1\times$  rotation frequency component with small order and large amplitude was retained, and the correction coefficient was approximately treated. Since the electromagnetic vibration of a motorized spindle is complex, and the rotor balancing cannot be reduced to 0 in practice, the balancing strategy can be accepted as long as its accuracy meets the requirements of the user. Therefore, the above approximations and simplifications are feasible, and the tested results prove this point. This idea is an exploration, and further research will be carried out in the future. The valuable conclusions of this paper are as follows:

(1) The mechanical and electromagnetic effects caused by rotor unbalance for a motorized spindle were introduced. Mechanical unbalance causes an inertia force, while electromagnetic unbalance induces an unbalanced magnetic pull (UMP). The UMP contains many components, whereas this work mainly focused on the  $1\times$  rotation frequency component affecting the frequency-domain adaptive balancing strategy. The derivation of UMP for a three-phase asynchronous squirrel-cage spindle motor was given, and, for a specific motorized spindle, the UMP and ratio of the air gap unbalance-induced  $1\times$  rotation frequency force component and the total  $1\times$  rotation frequency force were determined.

(2) Based on the study on UMP, a newly defined corrected coefficient for the improvement of the active balancing effect was defined. A frequency-domain adaptive balancing algorithm based on the corrected estimation scheme of the influence coefficient was built for motorized spindles.

(3) In order to validate the proposed balancing approach, a vibration test bed of a motorized spindle with a single electromagnetic ring balancer was developed. In the tests, two typical unbalance cases were designed, where displacement and acceleration sensors were used and the balancing tests were done at four different speeds. Finally, the balancing data under no balancing, conventional adaptive balancing, and the corrected adaptive balancing schemes were obtained. According to the analysis results, the proposed adaptive balancing approach was surely proven effective for the reduction of residual vibration after balancing for motorized spindles.

## 6. Patents

An invention patent from China was obtained (“On-line adaptive active balancing method for motorized spindle considering air gap unbalance” (No. ZL 201810162477.8)), in which a corrected adaptive balancing approach for motorized spindles considering the air gap unbalance was proposed.

**Author Contributions:** Conceptualization, H.F., M.J., H.L., and J.W.; methodology, J.W., H.F., and H.L.; validation, J.W. and M.J.; writing—original draft preparation, H.F.; writing—review and editing, S.S. and H.F.; funding acquisition, H.F. and X.Z. All authors read and agreed to the published version of the manuscript.

**Funding:** This research was funded by the National Natural Science Foundation of China (No. 51605380).

**Acknowledgments:** The authors thank Luoyang Bearing Science & Technology Co., Ltd of China for the motorized spindles used in this paper.

**Conflicts of Interest:** The authors declare no conflicts of interest.

## References

1. López de Lacalle, L.N.; Lamikiz, A. *Machine Tools for High Performance Machining*; Springer: London, UK, 2009; pp. 75–128.
2. Cao, H.R.; Zhang, X.W.; Chen, X.F. The concept and progress of intelligent spindles: A review. *Int. J. Mach. Tools Manuf.* **2017**, *112*, 21–52.
3. Urbikain, G.; Olvera, D.; López de Lacalle, L.N.; Elías-Zúñiga, A. Stability and vibrational behaviour in turning processes with low rotational speeds. *Int. J. Adv. Manuf. Technol.* **2015**, *80*, 871–885.
4. Urbikain, G.; Campa, F.J.; Zulaika, J.J.; López de Lacalle, L.N.; Alonso, M.A.; Collado, V. Preventing chatter vibrations in heavy-duty turning operations in large horizontal lathes. *J. Sound Vib.* **2015**, *340*, 317–330.
5. Urbikain, G.; Olvera, D.; López de Lacalle, L.N.; Elías-Zúñiga, A. Spindle speed variation technique in turning operations: Modeling and real implementation. *J. Sound Vib.* **2016**, *383*, 384–396.
6. Oleaga, I.; Pardo, C.; Zulaika, J.J.; Bustillo, A. A machine-learning based solution for chatter prediction in heavy-duty milling machines. *Measurement* **2018**, *128*, 34–44.
7. Liu, S.; Qu, L.S. A new field balancing method of rotor systems based on holospectrum and genetic algorithm. *Appl. Soft Comput.* **2008**, *8*, 446–455.
8. Xiang, S.T.; Yao, X.D.; Du, Z.C.; Yang, J.G. Dynamic linearization modeling approach for spindle thermal errors of machine tools. *Mechatronics* **2018**, *53*, 215–228.
9. Yang, A.S.; Yu, X.H.; Zhuang, J.R.; Lee, C.Y.; Hsieh, W.H. DOE-FEM based design improvement to minimize thermal errors of a high speed spindle system. *Therm. Sci. Eng. Prog.* **2018**, *8*, 525–536.
10. Abele, E.; Altintas, Y.; Brecher, C. Machine tool spindle units. *Cirp Ann. Manuf. Technol.* **2010**, *59*, 781–802.
11. Mikołajczyk, T.; Nowicki, K.; Bustillo, A.; Yu Pimenov, D. Predicting tool life in turning operations using neural networks and image processing. *Mech. Syst. Signal Process.* **2018**, *104*, 503–513.
12. Xul, J.; Zheng, X.H.; Zhang, J.J.; Liu, X. Vibration characteristics of unbalance response for motorized spindle system. *Procedia Eng.* **2017**, *174*, 331–340.
13. Deepthikumar, M.B.; Sekhar, A.S.; Srikanthan, M.R. Modal balancing of flexible rotors with bow and distributed unbalance. *J. Sound Vib.* **2013**, *332*, 6216–6233.
14. Bin, G.F.; Zhao, Q.L.; Jiang, Z.N.; Gao, J.J. Analysis of phase measurement based on influence coefficient and lag angle. *J. Vib. Meas. Diagn.* **2012**, *32*, 380–383. (In Chinese)

15. Chen, K.Y.; Tung, P.C.; Tsai, M.T.; Fan, Y.H. A self-tuning fuzzy PID-type controller design for unbalance compensation in an active magnetic bearing. *Expert Syst. Appl.* **2009**, *36*, 8560–8570.
16. Shchurova, A.V. Modeling of the turbine rotor journal restoration on horizontal balancing machines. *Procedia Eng.* **2016**, *150*, 854–859.
17. Shi, B.J.; Jing, M.Q.; Fan, H.W.; Wang, J.; Liu, H. Field balancing of grinding wheel spindle by single plane influence coefficient method. *Mach. Electron.* **2015**, *5*, 59–62. (In Chinese)
18. Rajalingham, C.; Bhat, R.B.; Rakheja, S. Automatic balancing of flexible vertical rotors using a guided ball. *Int. J. Mech. Sci.* **1998**, *40*, 825–834.
19. Vegte, J.V. Continuous automatic balancing of rotating systems. *J. Mech. Eng. Sci.* **1964**, *6*, 264–269.
20. Hredzak, B.; Guo, G. New electromechanical balancing device for active imbalance compensation. *J. Sound Vib.* **2006**, *294*, 737–751.
21. Fan, H.W.; Jing, M.Q.; Wang, R.C.; Liu, H.; Zhi, J.J. New electromagnetic ring balancer for active imbalance compensation of rotating machinery. *J. Sound Vib.* **2014**, *333*, 3837–3858.
22. Yun, X.L.; Mei, X.S.; Jiang, G.D.; Hu, Z.B.; Zhang, Z.H. Design and experimental research of a spray-type integrated online dynamic balance terminal. *J. Vib. Shock* **2019**, *38*, 79–84, 111 (In Chinese)
23. Gosiewski, Z. Automatic balancing of flexible rotors, Part I: Theoretical background. *J. Sound Vib.* **1985**, *100*, 551–567.
24. Gosiewski, Z. Automatic balancing of flexible rotors, Part II: Synthesis of system. *J. Sound Vib.* **1987**, *114*, 103–119.
25. Moon, J.D.; Kim, B.S.; Lee, S.H. Development of the active balancing device for high-speed spindle system using influence coefficients. *Int. J. Mach. Tools Manuf.* **2006**, *46*, 978–987.
26. Dyer, S.W.; Ni, J. Adaptive influence coefficient control of single-plane active balancing systems for rotating machinery. *J. Manuf. Sci. Eng.* **2001**, *123*, 291–298.
27. Kim, J.S.; Lee, S.H. The stability of active balancing control using influence coefficients for a variable rotor system. *Int. J. Adv. Manuf. Technol.* **2003**, *22*, 562–567.
28. Dyer, S.W.; Ni, J.; Shi, J.J.; Shin, K.K. Robust optimal influence-coefficient control of multiple-plane active rotor balancing systems. *J. Dyn. Syst. Meas. Control* **2002**, *124*, 41–46.
29. Fan, H.W.; Jing, M.Q.; Liu, H.; Yang, T.T. New machine tool motorized spindle integrated with one electromagnetic ring balancer driven by optimal square wave. *Proc. Inst. Mech. Eng. Part C J. Mech. Eng. Sci.* **2015**, *229*, 1509–1522.
30. Fan, H.W.; Zhi, J.J.; Shi, B.J.; Jing, M.Q.; Liu, H. Adaptive rotor balancing algorithm and single-disk rotation test for electromagnetic balancer. *J. Xi'an Jiaotong Univ.* **2018**, *52*, 15–21, 29. (In Chinese)
31. Fan, H.W.; Jing, M.Q.; Zhi, J.J.; Xin, W.H.; Li, M.; Liu, H. Development and validation of embedded control system for rotor online automatic balance. *J. Vib. Meas. Diagn.* **2015**, *35*, 746–751, 802. (In Chinese)
32. Fan, H.W.; Jing, M.Q.; Wu, T.Q.; Zhang, C.; Liu, H. Experimental study on influence of automatic balancer on dynamic performance of motorized spindle. *J. Test Meas. Technol.* **2013**, *27*, 369–376. (In Chinese).
33. Guo, D.; Chu, F.; Chen, D. The unbalanced magnetic pull and its effects on vibration in a three-phase generator with eccentric rotor. *J. Sound Vib.* **2002**, *254*, 297–312.
34. Chen, Y.X.; Zhu, Z.Q.; Ying, S.C. *Analysis and Control of Motor Noise*; Zhejiang University Press: Hangzhou, China, 1987; pp. 69–115. (In Chinese)
35. Wang, J. Study on Online Active Balance of Motorized Spindle Considering the Influence of Air-Gap Eccentricity. Master's Thesis, Xi'an Jiaotong University, Xi'an, China, 2016. (In Chinese)
36. Liu, Z.Z.; Yang, Z.J.; Xiao, L.; Yu, L.C. To analyze and calculate unilateral magnetic force of an induction motor. *J. Shandong Univ.* **2004**, *34*, 59–62. (In Chinese)
37. Zhang, C. Simulation Analysis and Experimental Study on Machine Tool Spindle. Master's Thesis, Xi'an Jiaotong University, Xi'an, China, 2013. (In Chinese)
38. Li, H.S.; Wu, S.; Kratz, H. FFT and wavelet-based analysis of the influence of machine vibrations on hard turned surface topographies. *Tsinghua Sci. Technol.* **2007**, *12*, 441–446.

